Wave packet dynamics of the $N(^4S)+O_2(X^3\Sigma_g^-)\rightarrow NO(X^2\Pi)+O(^3P)$ reaction on the X^2A' potential energy surface

Paolo Defazio and Carlo Petrongolo[a)]
Dipartimento di Chimica, Universita' di Siena, Via A. Moro, 53100 Siena, Italy

Stephen K. Gray
Chemistry Division, Argonne National Laboratory, Argonne, Illinois 60439

Carolina Oliva
Departament de Química Física i Centre de Recerca en Química Teòrica, Universitat de Barcelona, Martí i Franquès 1, 08028 Barcelona, Spain

(Received 20 February 2001; accepted 29 May 2001)

We report three-dimensional quantum calculations of total angular momentum $J=0$ reaction probabilities, *J*-shifting cross sections, and rate constants of the title reaction. Employing the real wave packet approach, we propagate wave packets corresponding to several $O_2(v,j)$ initial levels on the X^2A' potential surface of Sayós *et al.* As collision energy increases, the average probabilities first increase monotonically and then become nearly constant, while the cross sections rise in the overall energy range. Numerous probability resonances point out the formation of NOO collision complexes and NO final states. Rotational excitation in O_2 decreases the collisional energy thresholds and enhances the state-resolved rate constants, mainly at low temperature. O_2 vibrational excitation inhibits the reactivity, although the energy thresholds are still reduced. With respect to previous quasiclassical and mixed quantum-classical studies, we obtain lower thresholds and cross sections but similar rate constants, which are however lower than experimental rates. By inspection of the average properties of the wave packets, we suggest a qualitative reaction mechanism, we propose a modified *J*-shifting approximation, and we find a possible explanation of the low quantum reactivity on the present potential. © *2001 American Institute of Physics.*
[DOI: 10.1063/1.1386653]

I. INTRODUCTION

The reaction $N(^4S)+O_2(X^3\Sigma_g^-)\rightarrow NO(X^2\Pi)+O(^3P)$ plays an important role in atmospheric chemistry and in combustion processes, and is a good example of the reactivity of the ground-state N atom and of the formation of the ground electronic state of the NO molecule. At low enough energy, the reaction occurs adiabatically on the lowest two (X^2A' and a^4A') potential surfaces (PES) of the NO_2 molecule, which correlate to both reactants and products. The lowest (X^2A') PES has a deep well which supports thousands of bound states, while the first excited (a^4A') PES is unbound. The reaction is exoergic by 1.38 eV (Ref. 1) and has an activation energy of 0.28 eV.[2] The X^2A' and a^4A' barriers have C_s geometries and are[3,4] 0.27 and 0.65 eV, respectively. The NO_2 X^2A' zero-point energy is 4.50 eV below that of the reactants.[1,5]

Extensive experimental work on the kinetics of this reaction has measured the thermal rate constant in a wide temperature range.[2] As far as we know, detailed experimental studies of the reaction dynamics are rather few and report only the NO vibrational distribution at room temperature, with conflicting results.[6]

Theoretical studies of this reaction have employed analytical fits to *ab initio* PESs and statistical, quasiclassical, or approximate quantum-mechanical methods. Jaffe *et al.*,[7] Duff *et al.*,[4] and Bose and Candler[8] ran quasiclassical trajectories (QCT) on both doublet X^2A' and quartet a^4A' PESs and calculated cross sections, product vibrational distributions, and rate constants. Gilibert *et al.* obtained the same quantities via QCT (Ref. 9) or the reactive infinite-order sudden approximation[10] on the ground PES. Suzzi Valli *et al.*,[11] and Sayós *et al.*[3] (SHGG) reported variational-transition-state-theory (VTST) rate constants for the ground and both ground and quartet PESs, respectively. Finally, Balakrishnan and Dalgarno[12] used a (mixed) quantum-classical approach (QCA) for calculating cross sections and rate constants on both PESs.

Except the work by Suzzi Valli *et al.*,[11] the theoretical studies used four global X^2A' analytical PESs which correspond to different fits to the same set of *ab initio* data; the first is a London–Eyring–Polanyi–Sato surface[7] and the other three are of Sorbie–Murrell (SM) form.[3,6,9] The SM X^2A' PESs are qualitatively similar; all have C_s barriers of about 0.3 eV and C_{2v} barriers larger than 1.8 eV, and overestimate by about 3.3 eV the well depth which is also at a $D_{\infty h}$ geometry instead that at the experimental C_{2v} geometry. It has been argued[9] that this error should have a minor effect on the low-energy reaction dynamics, owing to the large C_{2v} barrier. The surface of Ref. 9 has also an artificial barrier of 0.55 eV,[4] which has been later removed in the improved SHGG surface. On the whole, the most recent X^2A' SHGG

a)Electronic mail: petro@hal.icqem.pi.cnr.it

TABLE I. Parameters of the calculations.[a]

Translational energy center of the initial wave packet	0.6 eV
R center and width of the initial wave packet	9 and 0.2
R range and No. of grid points	0–13.5 and 263
r range and No. of grid points	1.5–12.5 and 159
No. of Legendre polynomials	40 ($j''=1,3,...,79$)
No. of γ points	40 (using potential symmetry)
Potential and centrifugal cut-off	0.44
R and r absorption start at	10.5 and 9.5
R and r absorption strength	0.01
Flux analysis at r	8

[a]Values in a.u., unless otherwise specified.

potential seems to be the most accurate one because the corresponding VTST rate constants, also including the contribution from the $a\,^4A'$ surface, agree well with experiment.[3]

We report here the first three-dimensional, total angular momentum $J=0$ quantum dynamics study of the $N(^4S)+O_2(X\,^3\Sigma_g^-)\rightarrow NO(X\,^2\Pi)+O(^3P)$ reaction, based on the $X\,^2A'$ SHGG surface.[3] We also, unlike all previous work, properly account for the Pauli principle by including only odd $O_2(X\,^3\Sigma_g^-)$ rotational states. Standard J-shifting techniques[13] allow us to estimate reactive cross sections and thermal rate constants and compare with previous theoretical and experimental results. Despite the presence of three relatively heavy masses, interesting quantum effects, not present in the earlier theoretical calculations, are identified. Our quantum calculations, based on the real wave packet approach,[14] also allow inspection of the wave packet during the course of the reaction, thus allowing us to deduce a reaction mechanism. The wave packet formalism is described in Sec. II. Secs. III and IV present our results and the reaction mechanism, respectively, and Sec. V summarizes our conclusions.

II. METHODS

The method we use is well documented in previous publications[14–17] and it will only be sketched here. It starts[14] from a linearly scaled Hamiltonian $\hat{H}_s=a_s\hat{H}+b_s$, with eigenvalues in $(-1, 1)$, and is based on a $\cos^{-1}$ functional mapping of $\hat{H}_s$ and on a damped Chebyshev[18] recursive solution of the corresponding modified time-dependent Schrödinger equation (TDSE). Given a complex initial wave packet,[15] we propagate only its real part and obtain from it the total reaction probability.[14,16] Reactant Jacobi coordinates R, r, and γ are employed,[17] where R is the N–O_2 center-of-mass distance, r is the O–O distance, and γ is the angle between the vectors $\boldsymbol{R}$ and $\boldsymbol{r}$. For total angular momentum quantum number $J=0$, the Hamiltonian and the wave packet are represented in an evenly spaced grid of radial coordinates and in a basis of normalized Legendre polynomials $P_{j''}(\cos\gamma)$. Because the ^{16}O nuclear spin is zero and the O_2 electronic state is $X\,^3\Sigma_g^-$, j'' is an odd quantum number in agreement with the Pauli principle.[19] The real part of the wave packet is thus written as

$$q^k(R,r,\cos\gamma)=\sum_{j''} C^k_{j''}(R,r)\overline{P}_{j''}(\cos\gamma), \tag{1}$$

where k labels the recursion number.

Within the real wave packet formalism, Eq. (1) represents the real part of the exact solution of the modified TDSE with the Hamiltonian operator $\hat{H}$ replaced by $f(\hat{H})=-(1/\tau)\cos^{-1}\hat{H}_s$ in atomic units, $i\partial\psi'(t')/\partial t'=f(\hat{H})\psi'(t')$ ($t'=k\tau$, where τ is an arbitrary step size that cancels out of any expression for an energy resolved observable). It is important to realize that $\psi'(t')$ can also be approximately related to solutions of the ordinary TDSE, as sketched out in Ref. 15. In particular, if one considers $f(E)$, the eigenvalue spectrum of $f(\hat{H})$, one can expand it in a first order Taylor series about the mean wave packet energy $\overline{E}$: $f(E)\approx f(\overline{E})+(df/dE)_{\overline{E}}(E-\overline{E})$. Replacing E with $\hat{H}$ yields a linear approximation to $f(\hat{H})$: $f(\hat{H})\approx f(\overline{E})+(df/dE)_{\overline{E}}(\hat{H}-\overline{E})$. Because, in comparison with the entire range of energies E, the wave packet occupies a relatively narrow region of energies about $\overline{E}$, this approximation is quite good. However, it is a simple exercise to show that any wave packet satisfying a TDSE of the form $i\partial\psi'(t')/\partial t'=(A\hat{H}+B)\psi'(t')$ is related to a wave packet satisfying the usual TDSE if $\psi'(t'=0)=\psi(t=0)$. In particular, $\psi(t)=\exp(iBt/A)\,\psi'(t'=t/A)$. Apart from an insignificant phase factor, one can thus relate the physical wave packet $\psi(t)$ to the wave packet $\psi'(t')$ evolving under the modified TDSE by simply evaluating $\psi'(t')$ at $t'=t/A$. This implies that physical times are related to t' (which is effectively the recursion number k) by $t=At'$. This leads to[15] $t\approx\hbar k a_s/(1-E_s^2)^{1/2}$, where E_s is the mean energy of the wave packet expressed in the scaled energy system, $E_s=a_sE+b_s$. These observations also allow us to attach approximate physical significance to the evolution of the expectation values of R, r, and $\cos\gamma$; apart from some extra, high frequency oscillations owing to use of just the real part of $\psi'(t')$, these expectation values will be very close to the actual expectation values calculated from a complex wave packet $\psi(t)$.

The necessary matrix-vector products are calculated via R and r fast sin Fourier transforms and a γ discrete variable representation. As usual, the wave packet is damped at the radial grid edges. Our completely rigorous dynamical calculations are restricted to total angular momentum $J=0$. Initial wave packets corresponding to incoming Gaussians in R and various rovibrational states v, j of $O_2(X\,^3\Sigma_g^-)$ are propagated in the manner described, and a flux analysis[16] at a suitable r value separating reactants from products is carried out to obtain the total reaction probability, $P^{J=0}_{v,j}$. Table I reports the parameters of the initial wave packet, of the Chebyshev propagation, and of the probability calculation. With these parameters, the collisional energy range is about from 0.2 to 1.2 eV, and the propagation time step is 0.04 fs.

The flux analysis converges essentially the reaction probability in about 40 000 steps, but we iterate up to 80 000 steps (~3.334 ps), in order to converge the fine features of the reaction probability. The final norm shows that 99.7% of the wave packet has been absorbed and the probability calculated via the flux method agrees within 10% with that

obtained from the asymptotic analysis of Ref. 13 (we report only the flux-based results, which we believe to be more accurate than the asymptotic-analysis results, especially in the low collision energy limit). As with most wave packet methods, once the wave packet has been propagated and the relevant information saved, we can construct the reaction probability for any (continuous) energy contained within the energy spread of the wave packet. Of course, in practice a dense grid of energies is used. We have calculated reaction probabilities at 200 $E_{\rm col}$ values in the 0.2–1.2 eV energy range, and we have checked the results by considering 2000 $E_{\rm col}$ values in some cases, i.e., an energy step much smaller than the widths of the probability oscillations.

If K is the total angular momentum quantum number along $\boldsymbol{R}$, we use the J-shifting (JS) approximation[13,20] to estimate the probabilities $P^J_{vjK}(E_{\rm col})$ at $J>0$, collision energy $E_{\rm col}$, and from an $O_2|vjK\rangle$ initial state. In this approximation K is assumed to be a good quantum number and

$$P^J_{vjK}(E_{\rm col}) \approx P^0_{vj0}(E_{\rm col} - E^{J\neq}_K), \tag{2}$$

where $E^{J\neq}_K$ is the rotational energy of the rigid transition state (TS). For $N+O_2$, the TS geometry[3] is $R^{\neq} = 4.1994$ bohr, $r^{\neq} = 2.2960$ bohr, and $\gamma^{\neq} = 54.12°$, and the corresponding rotational constants $A^{\neq}$, $B^{\neq}$, and $C^{\neq}$ are 2.39, 0.32, and 0.28 $\rm cm^{-1}$, respectively. The TS is thus a nearly prolate symmetric top with

$$E^{J\neq}_K \approx \overline{B}^{\neq} J(J+1) + (A^{\neq} - \overline{B}^{\neq})K^2, \tag{3}$$

where $\overline{B}^{\neq}$ is the average of $B^{\neq}$ and $C^{\neq}$.

We then calculate the degeneracy-averaged cross sections $\sigma_{vj}(E_{\rm col})$ with the usual BF partial wave sum,[21] and from them the state-resolved rate constants[22] $k_{vj}(T)$ as appropriate Boltzmann averages over the collision energy and cross section,[23] by including the electronic degeneracy 1/6. Finally, proper thermal rate constants $k(T)$ are obtained by summing the $k_{vj}(T)$ over all relevant reactant states with the appropriate internal reactant state energy Boltzmann weights. The full thermal rate constant $k(T)$ has been obtained by using explicitly $v=0$, 1, and 2 and j up to 11, 5, and 1, respectively, and by assuming that $k_{0,j>11} \approx k_{0,11}$, $k_{1,j>5} \approx k_{1,5}$, and $k_{2,j>1} \approx k_{2,1}$. We focus on rate constants with $T < 1500$ K for which the contribution to the rate from dynamics on the first excited state is quite small. At $T=1500$, for example, the results of Ref. 3 suggest that the excited state contributes 10% to the rate constant, and for $T \leqslant 1000$ K its contribution is less than 3%.

III. PROBABILITIES, CROSS SECTIONS, AND RATE CONSTANTS

Figures 1 and 2 show the total reaction probabilities $P^0_{vj}(E_{\rm col})$ from all O_2 initial states we have investigated. The collisional energy threshold of the O_2 ground rovibrational state ($v=0$ and $j=1$) is ~0.34 eV, corresponding to a total energy of ~0.44 eV. This value is larger than the potential barrier, and shows that the reaction occurs without an appreciable tunnel effect and that the relevant energetic wave packet components probe potential regions more repulsive than the minimum energy path (MEP). The threshold and the

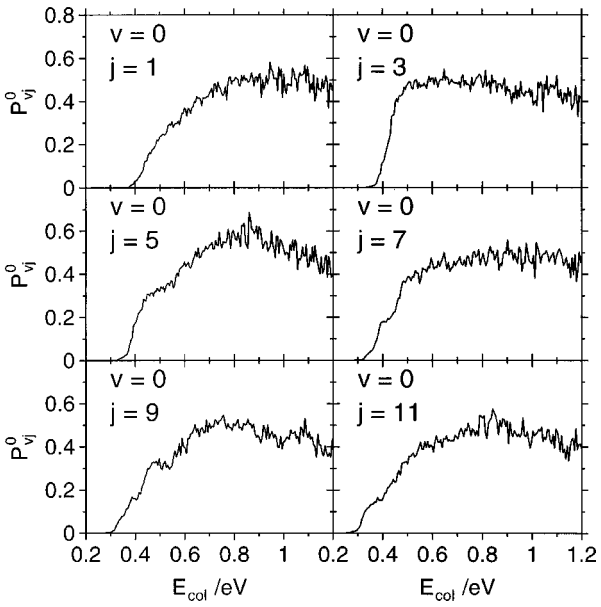

FIG. 1. Total probabilities P^0_{0j} vs collision energy for $N+O_2(v=0,j) \rightarrow NO+O$.

fast initial increase of the probability are consistent with an activated and direct process at low collision energies, ≤0.45–0.65 eV, depending on v and j. When O_2 is rotationally excited, the collisional threshold decreases up to ~0.27 eV at $v=0$ and $j=11$ (total energy ~0.39 eV), and the low-energy reaction probability is strongly enhanced. At higher collision energies the reaction is not longer direct; the probability has indeed many sharp resonances superimposed on a broad continuum, owing to the formation of many short-lived NOO collision complexes which then dissociate into various v', j' product channels. The largest reaction probability is equal to 0.69 at $E_{\rm col}=0.86$ eV for $v=0$ and $j=5$. At high collision energy, the average probabilities eventually attain nearly constant values between 0.4 and 0.5. This behavior points out important recrossing effects with a strong competition between reactive and nonreactive collisions.

The comparison between Figs. 1 and 2 shows a general reactivity decrease upon increasing the O_2 vibrational exci-

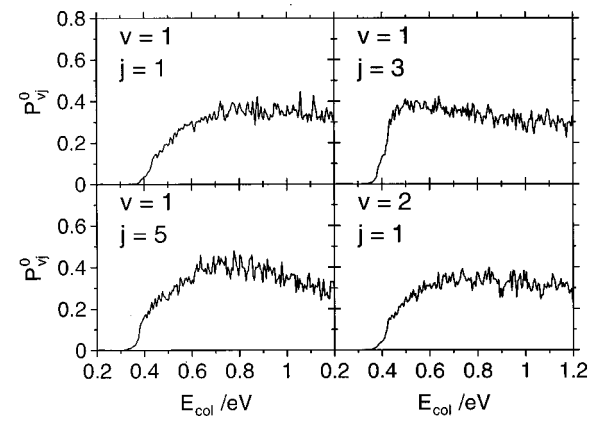

FIG. 2. Total probabilities P^0_{1j} and P^0_{2j} vs collision energy for $N+O_2(v=1 \text{ or } 2,j) \rightarrow NO+O$.

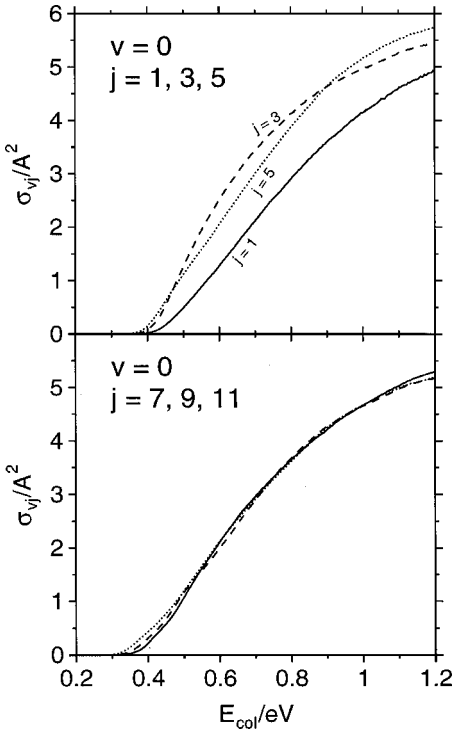

FIG. 3. Degeneracy-averaged JS cross sections σ_{0j} vs collision energy for $N+O_2(0,j)\rightarrow NO+O$. In the lower part of the figure, full, dashed, and dotted lines refer to $j=7$, 9, and 11, respectively.

tation, probably because the corresponding wave packets spread on more repulsive potential regions and the reaction is thus inhibited.

The JS reaction cross sections $\sigma_{vj}(E_{\mathrm{col}})$ of Figs. 3 and 4

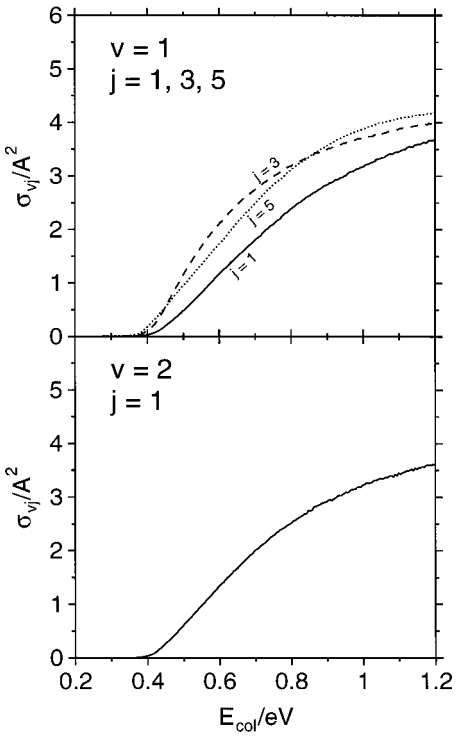

FIG. 4. Degeneracy-averaged JS cross sections σ_{1j} and σ_{2j} vs collision energy for $N+O_2(v=1 \text{ or } 2,j)\rightarrow NO+O$.

show similar trends to those of the reaction probabilities, except that all resonances are smoothed by the partial wave expansion. Note the reactivity inversion from $j=3$ to $j=5$ between about 0.45 and 0.85 eV, and the nearly equal values of the cross sections at $j=7$, 9, and 11. As expected, many J values contribute to the cross sections: for $v=0$ and $j=1$, e.g., the partial wave expansion includes J values up to 72, 126, and 163 at $E_{\mathrm{col}}=0.4$, 0.8, and 1.2 eV, respectively.

There are some previous theoretical results for the reactive cross section[8,12] that we can compare to. These results focused on the $v=0$, $j=8$ cross section, which if the Pauli principle were ignored would be the most populated reactant state at $T=300$ K. As we already pointed out, only odd j reactant states can exist for the ground electronic state of O_2. However, we do not see much variation between our $v=0$ cross sections with $j=7$, 9, and 11 (Fig. 3) and so we can compare our results with the previous theoretical ones. The QCT results of Ref. 8 correspond to a different PES than the one we employ, namely to that by Duff *et al.*,[4] but QCA results[12] based on the present SHGG (Ref. 3) surface are in reasonable agreement with the QCT results (see Fig. 1 of Ref. 12). Our reaction thresholds for $v=0$ and $j=7$ or 9 are ~0.28 eV, smaller than the QCT and QCA thresholds. However, the magnitudes of our cross sections tend to be a bit lower at energies above threshold and more dependent on v and j. For example, at $E_{\mathrm{col}}=1$ eV, the QCA cross section is ~6.3 Å^2, whereas our cross section is ~4.7 Å^2, 25% lower. We also differ from the QCA (Ref. 12) results in relation to the effect of reactant vibrational excitation; we find a decrease in the cross section (compare Figs. 3 and 4) when $v=1$ is considered, whereas the QCA results suggest a slight increase. It is difficult to explain the origins of these differences and two possible reasons are: (i) The artificial and deep $D_{\infty h}$ hole of the SHGG surface[3] which yields many NOO quantum resonances, which would not be well described by the QCT or even the QCA methods. These resonances could inhibit the reactivity; we shall discuss this hypothesis in Sec. IV. (ii) The inaccuracy of the JS approximation, which depends on the geometry of the reaction bottleneck. This approximation is likely to become more in error with increasing J, j, and collision energy. However, this hypothesis does not obviously explain why the cross section discrepancies occur over a wide range of E_{col}. We will address these two possibilities in Sec. IV.

Our v and j initial-state-resolved rate constants $k_{vj}(T)$ increase strongly with j at low temperature. For example, $k_{0,1}(300)=1.5\times10^{-18}\,\mathrm{cm^3\,s^{-1}}$ and $k_{0,11}(300)=1.5\times10^{-17}\,\mathrm{cm^3\,s^{-1}}$, whereas they are less j dependent at 1500 K. Table II shows that our thermal rate constant $k(T)$ is underestimeted with respect to both experimental[2] and VTST (Ref. 3) data, although the difference decreases at high T. On the other hand, QCT (Ref. 8) and QCA (Ref. 12) calculations give rate constants similar to ours. Thus QCT, QCA, and quantum dynamical theories are in satisfactory agreement among themselves but are yielding quite different results than VTST at low T.

This agreement implies that the wrong NO_2 minimum of the fitted PESs (Refs. 3, 4) affects the reaction dynamics, contrary to previous assumptions.[9] On the other hand, the

TABLE II. Temperature in K and rate constants in $cm^3\,s^{-1}$.

T	Expt.[a]	VTST[b]	QCT[c]	QCA[d]	This work[e]
300	$(8.3\pm0.1)\times10^{-17}$	8.7×10^{-17}	5.5×10^{-18}	1.0×10^{-17}	$0.95-1.0\times10^{-17}$
600	$(3.9\pm0.1)\times10^{-14}$	3.2×10^{-14}	9.9×10^{-15}	1.0×10^{-14}	$8.9-9.9\times10^{-15}$
1000	$(5.7\pm0.3)\times10^{-13}$	4.2×10^{-13}	2.6×10^{-13}	2.2×10^{-13}	$1.8-2.0\times10^{-13}$
1500	$(2.5\pm0.3)\times10^{-12}$	1.8×10^{-12}	1.6×10^{-12}	1.5×10^{-12}	$0.92-1.0\times10^{-12}$

[a]Best fit of Ref. 2.
[b]PES of Ref. 3.
[c]PES of Ref. 4 and Eq. (6) of Ref. 8.
[d]PES of Ref. 3. Estimated from Fig. 4 of Ref. 12.
[e]PES of Ref. 3. The two values correspond to the TS of the PES or to the effective TSs, respectively (see Sec. IV).

accord between VTST and experiment shows that the SHGG surface is correct in the barrier region which is most important in VTST calculations.

IV. REACTION MECHANISM

Qualitative insights into the reaction mechanism are obtained from the inspection of Figs. 5 and 6 which show, respectively, the radial trajectory and the γ averaged probability density

$$\rho(R,r,t)=\sum_{j''}|C_{j''}(R,r,t)|^2, \tag{4}$$

when O_2 is initially in its ground rovibrational state ($v=0$, $j=1$). The trajectory and the density are superimposed on the plot of the PES at $\gamma=54.12°$, the value of the Jacobi angle at the potential barrier. The expectation value of $\cos\gamma$ is zero by symmetry. We have however calculated the expectation value $\langle|\cos\gamma|\rangle$ and from that we have estimated an average angle $\overline{\gamma}=\cos^{-1}\langle|\cos\gamma|\rangle$.

The expectation values of the radial coordinates attain nearly constant values after about 400 fs. Likewise, $\overline{\gamma}$ undergoes some oscillations between 36° and 59° in the first 175 fs and then is practically constant in time and equal to about 49°. These constant values of the average nuclear coordinates do not imply that the reaction is over so quickly, because more than 3.3 ps are necessary for converging the reaction probability, but simply point out that the wave packet is so delocalized after 400 fs that the average nuclear coordinates do not vary appreciably.

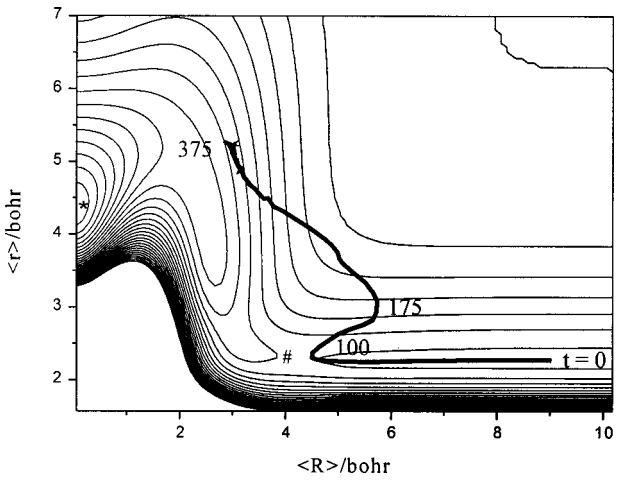

FIG. 5. Radial trajectory for $v=0$ and $j=1$, superimposed on the plot of the PES at $\gamma=54.12°$. The energy zero is at $N+O_2(r^{eq})$. The barrier is at 0.27 eV and is denoted by #. The NO_2 $D_{\infty h}$ minimum is at -7.96 eV and is denoted by *. Contour levels start from 5.2 eV at the right upper corner and their spacing is 0.83 eV. Time t in fs.

The expectation values of the nuclear coordinates and the snapshots of the probability density show qualitatively that the reaction occurs via a three-step mechanism in the first 400 fs. (1) The wave packet is initially well localized in the $N+O_2$ reactant channel and it then moves towards the interaction region. Up to about 100 fs, N approaches O_2 which remains practically unperturbed, and the average position of the wave packet reaches the region of the potential barrier at about 100 fs. (2) Between 100 and 175 fs, the wave packet is partly reflected back by the repulsive wall of the potential and thus $\langle R\rangle$, $\langle r\rangle$, and the average N–O distances increase. In this time interval, a large part of the wave packet comes back into the reactant channel and a minor part moves into the NO_2 minimum region. (3) Between 175 and 375 fs, the linear potential well captures part of the wave packet and thus $\langle R\rangle$ decreases and the small-R density grows. The reaction now occurs via a partial C_s insertion mechanism, with formation of short-lived NOO complexes: the $\langle r\rangle$ distance between the O atoms increases while the N atom approaches one O atom. At larger times, the NOO complexes eventually break down giving the NO+O products. The highly fragmented, complex behavior of the wave packet, evident in the interaction region for $t\geqslant175$ fs in Fig. 6, is symptomatic of dense, probably overlapping resonances playing a role in the dynamics. See, for example, studies of the $O(^1D)+H_2$ reaction[15] and of the $H+O_2$ reaction.[24,25]

This scenario is coherent with the probability results, although it is merely qualitative because relies on the average position and snapshots of the real part of a modified wave packet which moreover delocalizes as time increases. At $t>400$ fs, the wave packet is so delocalized that it is impossible to estimate even a qualitative reaction mechanism. However, the modified wave packet is a good approximation to the more physically meaningful one that satisfies the usual TDSE (Ref. 17) and its analysis allows to estimate a reliable reaction mechanism.

This reaction mechanism allows us to explain why the quantum cross sections are lower than those QCA (Ref. 12) on the same potential.[3] The inspection of Figs. 5 and 6 shows indeed a monotonic descending energy path from the PES barrier (#) to the NO_2 $D_{\infty h}$ PES minimum (*), and that a

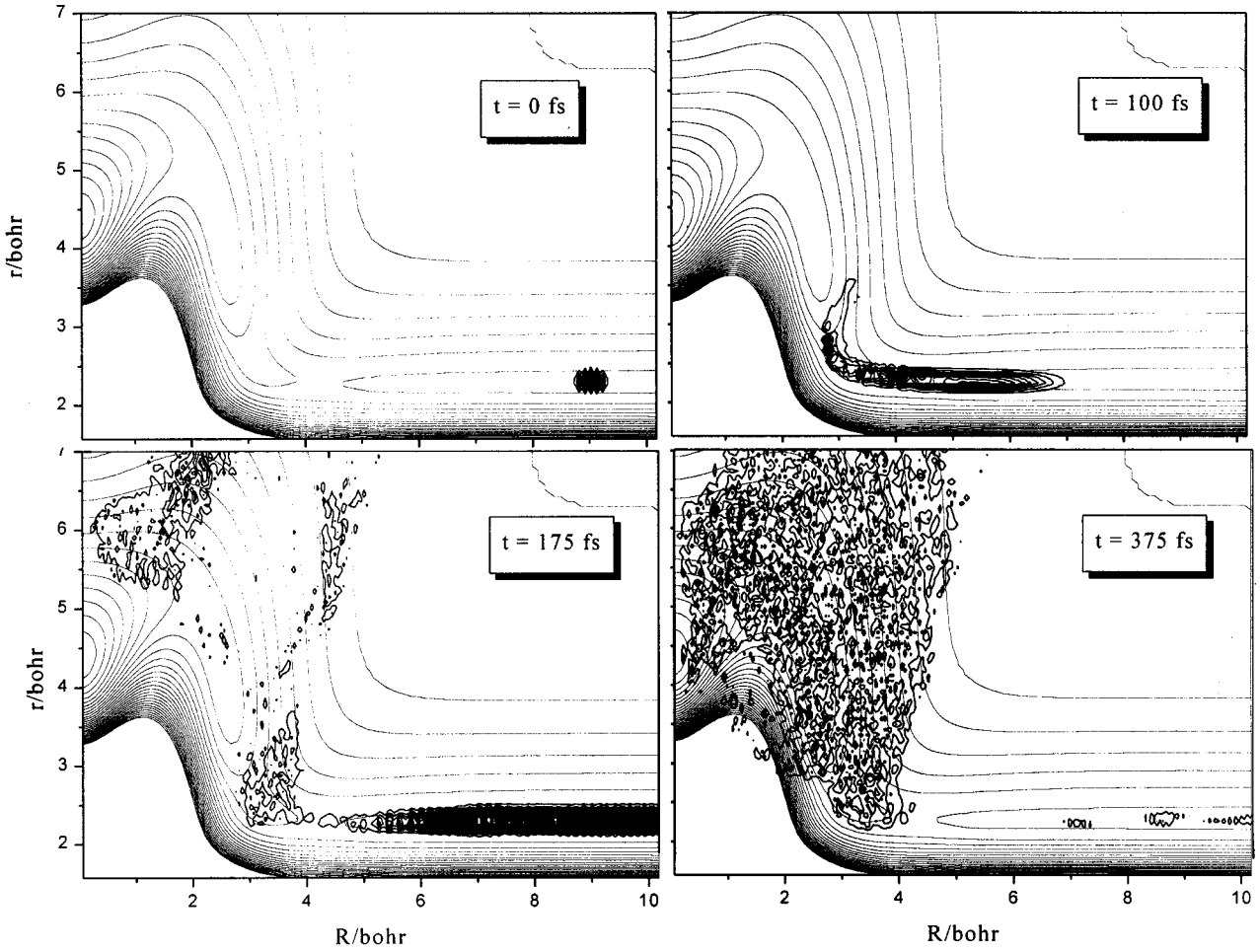

FIG. 6. Wave packet density for $v=0$ and $j=1$ at four times, superimposed on the plot of the PES at $\gamma=54.12°$.

portion of the wave packet thus enters into this nonreactive potential region. This mechanism lowers the quantum reactivity and is ruled by the translational R coordinate. Moreover, the decrease of the cross sections when O_2 is vibrationally excited can be explained by a vibrational-to-translational energy redistribution which pushes further the wave packets into the nonreactive potential hole. We therefore suggest that these quantum effects are not accounted for by QCA (Ref. 12) which describes classically the relevant motion along R. In conclusion, the three-dimensional quantum dynamics is very sensitive to the shape of the attractive region of the PES, in contrast to previous calculations.

On the basis of the above mechanism, we also propose a modified JS approximation which relies on variable TS geometries in Eq. (3). Indeed, Figs. 5 and 6 point out that the wave packet feels an effective potential barrier at about 100 fs, when it is reflected back by the potential. The geometry of this effective TS is rather shifted from the PES bare TS, and depends on the translational energy center and vibrorotational quantum numbers of the initial wave packet. By employing the geometry values of these effective barriers in Eq. (3), our cross sections and rate constants increase by about 12%, thus reducing the gap from the QCA ones[12] based on the same SHGG PES. The last column of Table II shows both standard-JS and modified-JS rate constants.

V. CONCLUSIONS

This paper describes the first quantum calculations for an important reaction consisting of three heavy nuclei, namely, $N(^4S)+O_2(X\,^3\Sigma_g^-)\rightarrow NO(X\,^2\Pi)+O(^3P)$. We employed the Sayós *et al.*[3] $X\,^2A'$ adiabatic PES, which has a correct barrier in the entrance channel but a too deep minimum at a $D_{\infty h}$ geometry. We used a wave packet mehod[14] coupled with flux analysis[16] to infer accurate $J=0$ reaction probabilities, including all three internal nuclear coordinates. We investigated a variety of $O_2(v,j)$ initial states, where j is an odd quantum number in agreement with the Pauli principle. Reaction cross sections and rate constants were then obtained within the framework of the standard JS approximation.[13,20] We also suggested a reaction mechanism and a modified JS approximation based on this mechanism.

At short times and low collision energies, the reaction proceeds via a direct mechanism, corresponding to the approach of the N atom to the unperturbed O_2 diatom, and to a monotonic increase of the reaction probability. At larger times we see a partial insertion mechanism due to some trapping of the wave packet into the strong interaction region of the PES. At high collisional energies, this mechanism yields many resonances in the probability, due to the formation of metastable NOO intermediates and to the opening of

$NO(v',j')$ product channels. In this limit, the probability averaged over small collision energy windows becomes nearly constant. The O_2 rotational excitation increases in general the reactivity, whereas the O_2 vibrational excitation has an opposite effect.

The comparison with previous quasiclassical[8] and mixed quantum-classical[12] studies points out the new results of our work and some interesting quantum effects. The present time-dependent method yields indeed all the detailed energy dependence of the reaction probability, including many probability resonances. We obtain smaller reaction thresholds and cross sections than those of Refs. 8 and 12, and our quantum calculations show the importance of the $D_{\infty h}$ NO_2 minimum in the microscopic reaction mechanism. We have indeed shown that this nonreactive potential region captures part of the wave packet, thus enhancing the formation of reaction intermediates and lowering the overall reactivity. The present and previous calculated rate constants[8,12] are in good agreement, although all underestimate the experimental data.[2] On the basis of the reaction mechanism, we ascribe this result to the uncorrect shape of the Sayós *et al.*[3] and Duff *et al.*[4] PESs in the NO_2 bound region, rather than to a too large potential barrier. Further work is currently in progress for checking this hypothesis.

ACKNOWLEDGMENTS

We thank Professor R. Sayós for providing us with his PES code and parameters, and for many helpful discussions. This work has been supported by the MURST (Programmi di Ricerca Scientifica di Rilevante Interesse Nazionale), by the CNR (Progetti Coordinati), and by the University of Siena (Progetti di Ricerca). One of the authors (C.P.) thanks the hospitality of the ICQEM-CNR, Pisa. (S.K.G.) was supported by the Office of Basic Energy Sciences. Division of Chemical Sciences, U.S. Department of Energy, under Contract No. W-31-109-ENG-38. (C.O.) thanks the Spanish Ministry of Culture and Education for a predoctoral visiting grant at the University of Siena, within the research project PB98-1209-C02-01.

[1] K. P. Huber and G. Herzberg, *Constants of Diatomic Molecules* (Van Nostrand, New York, 1979).
[2] D. L. Baulch, C. J. Cobos, R. A. Cox, G. Hayman, T. Just, J. A. Kerr, T. Murrells, M. J. Pilling, J. Troe, R. W. Walker, and J. Warnatz, J. Phys. Chem. Ref. Data **23**, 847 (1994), and references therein.
[3] R. Sayós, J. Hijazo, M. Gilibert, and M. González, Chem. Phys. Lett. **284**, 101 (1998).
[4] J. W. Duff, F. Bien, and D. E. Paulsen, Geophys. Res. Lett. **21**, 2043 (1994).
[5] R. Jost, J. Nygard, A. Pasinski, and A. Delon, J. Chem. Phys. **105**, 1287 (1996).
[6] I. C. Winkler, R. A. Stachnik, J. I. Steinfeld, and S. M. Miller, J. Chem. Phys. **85**, 890 (1986), and references therein.
[7] R. L. Jaffe, M. D. Pattengill, and D. W. Schwenke, in *Supercomputer Algorithms for Reactivity, Dynamics, and Kinetics of Small Molecules*, edited by A. Lagana (Kluwer, Dordrecht, 1989), p. 367.
[8] D. Bose and G. V. Candler, J. Chem. Phys. **107**, 6136 (1997).
[9] M. Gilibert, A. Aguilar, M. González, and R. Sayós, Chem. Phys. **172**, 99 (1993).
[10] M. Gilibert, X. Giménez, M. González, R. Sayós, and A. Aguilar, Chem. Phys. **191**, 1 (1995).
[11] G. Suzzi Valli, R. Orrú, E. Clementi, A. Lagana′, and S. Crocchianti, J. Chem. Phys. **102**, 2825 (1995).
[12] N. Balakrishnan and A. Dalgarno, Chem. Phys. Lett. **302**, 485 (1999).
[13] J. M. Bowman, J. Phys. Chem. **95**, 4960 (1991).
[14] S. K. Gray and G. G. Balint-Kurti, J. Chem. Phys. **108**, 950 (1998).
[15] G. G. Balint-Kurti, A. I. Gonzales, E. M. Goldfield, and S. K. Gray, Faraday Discuss. **110**, 169 (1998).
[16] A. J. H. M. Meijer, E. M. Goldfield, S. K. Gray, and G. G. Balint-Kurti, Chem. Phys. Lett. **293**, 270 (1998).
[17] S. K. Gray, E. M. Goldfield, G. C. Schatz, and G. G. Balint-Kurti, Phys. Chem. Chem. Phys. **1**, 1141 (1999).
[18] V. A. Mandelshtam and H. S. Taylor, J. Chem. Phys. **103**, 2903 (1995).
[19] G. Herzberg, *Molecular Spectra and Molecular Structure* (Krieger, Malabar, Florida, 1989), Vol. I, p. 251.
[20] H. Koizumi, G. C. Schatz, and M. S. Gordon, J. Chem. Phys. **95**, 6421 (1991).
[21] R. T. Pack, J. Chem. Phys. **60**, 633 (1974).
[22] R. D. Levine and R. B. Bernstein, *Molecular Reaction Dynamics and Chemical Reactivity* (Oxford University Press, New York, 1987), p. 179.
[23] S. K. Gray, C. Petrongolo, K. Drukker, and G. C. Schatz, J. Phys. Chem. A **103**, 9448 (1999).
[24] D. H. Zhang and J. Z. H. Zhang, J. Chem. Phys. **101**, 3671 (1994).
[25] R. T. Pack, E. A. Butcher, and G. A. Parker, J. Chem. Phys. **102**, 5998 (1995).